


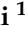


Article

Mechanochemical Synthesis and Hydrogen Sorption Properties of a V-Ni Alloy

Oriele Palumbo ¹, Nicholas Carboni ¹, Francesco Trequattrini ², Sergio Brutti ^{1,3} and Annalisa Paolone ^{1,*}

¹ Consiglio Nazionale delle Ricerche, Istituto dei Sistemi Complessi, Piazzale Aldo Moro 5, 00185 Rome, Italy; oriele.palumbo@roma1.infn.it (O.P.); carboni.1718048@studenti.uniroma1.it (N.C.); sergio.brutti@uniroma1.it (S.B.)

² Department of Physics, Sapienza University of Rome, Piazzale Aldo Moro 5, 00185 Rome, Italy; francesco.trequattrini@roma1.infn.it

³ Department of Chemistry, Sapienza University of Rome, Piazzale Aldo Moro 5, 00185 Rome, Italy

* Correspondence: annalisa.paolone@roma1.infn.it

Abstract: Vanadium can store large quantities of hydrogen (about 4 mass%). However, only half of it can be reversibly absorbed. To avoid this issue, various partial substitutions were previously proposed, such as Ni. In this work, we explore the synthesis of a $V_{85}Ni_{15}$ alloy by means of ball milling, a simpler and more scalable method compared to arc or induction melting usually applied for metal alloys. After ball milling the powders of the pure metals for 15 h in argon, SEM–EDX measurements confirmed the stoichiometry of the synthesized material, which has a typical particle dimension of the order of a few microns and is composed from the coalescence of nanometric primary particles. XRD indicated a BCC crystalline structure with a typical grain size of ≈ 3 nm. Hydrogen can be absorbed without activation procedures at high temperatures. Up to $H/M \approx 0.08$, one can observe the occurrence of a solid solution of hydrogen in the alloy, while at a higher hydrogen content, the formation of a hydride is likely to occur. The maximum hydrogen content is $H/M \approx 0.4$ at the maximum investigated pressure in this study of $p \approx 45$ bar. Both the hydrogenation enthalpy and entropy decrease as the hydrogen content increases, and the shape of the sorption isotherms is different from that of $V_{85}Ni_{15}$ produced by induction melting, possibly because of the nanometric dimensions of the particles produced by ball milling.

Keywords: ball milling; vanadium alloys; hydrogen storage; SEM–EDX; X-ray diffraction; pressure-composition isotherms



Citation: Palumbo, O.; Carboni, N.; Trequattrini, F.; Brutti, S.; Paolone, A. Mechanochemical Synthesis and Hydrogen Sorption Properties of a V-Ni Alloy. *Hydrogen* **2022**, *3*, 112–122. <https://doi.org/10.3390/hydrogen3010009>

Academic Editor: George E. Marnellos

Received: 30 December 2021

Accepted: 25 February 2022

Published: 2 March 2022

Publisher's Note: MDPI stays neutral with regard to jurisdictional claims in published maps and institutional affiliations.



Copyright: © 2022 by the authors. Licensee MDPI, Basel, Switzerland. This article is an open access article distributed under the terms and conditions of the Creative Commons Attribution (CC BY) license (<https://creativecommons.org/licenses/by/4.0/>).

1. Introduction

Pure vanadium can store large quantities of hydrogen, as it can reach the composition of the dihydride, VH_2 . Due to the relatively low mass of vanadium, VH_2 has a high storage capacity of about 4 mass%, which can also be reached at room temperature [1]. However, only about half of it can be reversibly absorbed/desorbed, as the V-H system has a peculiar and complex phase diagram [1,2]. In fact, vanadium has three stable hydrides, with compositions $VH_{0.5}$, VH and VH_2 [1,2]. When measuring the pressure composition isotherms, one can observe various pressure plateaus; however, the one corresponding to the transition from the solid solution (α phase) to $VH_{0.5}$ has an extremely low pressure, on the order of 1 mbar [3,4]; therefore, it is extremely difficult to remove hydrogen at low hydrogen concentrations. One way to partially mitigate the irreversible storage of hydrogen in vanadium is the partial substitution of V with other metals, such as Ti, Cr, Ni, Fe, etc., which generally leads to a higher equilibrium pressure and a sloping plateau [3,5–7] in the pressure composition isotherms.

Vanadium also displays one of the highest diffusion coefficients for hydrogen [8], making this metal attractive for the production of membranes for hydrogen purification [9,10].

However, the high solubility of hydrogen in vanadium tends to make it brittle and pulverizes it upon hydrogen absorption/desorption. The partial substitution of V with other metals was also proposed [9] to avoid this drawback.

Recently, we investigated a $V_{85}Ni_{15}$ alloy produced by induction melting, regarding its hydrogen and deuterium sorption properties [11,12]. It must be noted that the V-H and V-D systems have clear different phase diagrams, and this fact is also reflected in the $V_{85}Ni_{15}$ alloy [11,12]. Moreover, this V-Ni alloy also has very fast absorption/desorption kinetics, suggesting that this material is a good candidate also for hydrogen purification [11,12].

The procedure to synthesize this sample required several steps in a vacuum induction melting apparatus: firstly, a $V_{65}Ni_{35}$ alloy was melted at 1380 °C; then, the liquid was heated at 1800 °C and the required quantity of pure V was added to reach the desired composition [11]. Induction furnaces and arc melting are the most commonly used means to synthesize metal alloys. In this work, we aimed to explore the possibility of using ball milling to produce a V-Ni alloy, as this last method certainly requires both less equipment and time. Indeed, ball milling has been largely used for the production of hydrides or materials to be hydrogenated [13–15]. More than 20 years ago, the use of ball milling revolutionized the field of hydrogen storage and opened the ground for the search and use of new hydrides [13]. Ball milling allows for the incorporation of catalysts to facilitate the kinetics of sorption and the decrease in the dimensions of the powders, so that the diffusion processes of hydrogen can occur much easier and faster [14,15]. Moreover, this method allows for the production of materials around room temperature, avoiding possible decompositions at higher temperatures [14].

Some reports on the ball milling of V and V alloys are available. Orimo et al. produced VH_x ($0.67 < x < 0.82$, depending on the milling time) in a reactive ball milling at room temperature, using a pressure of hydrogen of about 1 MPa [16]. Incidentally, these authors showed that the grain size can reach values as low as 10 nm, but the system does not reach an amorphous state [16]. Krishnan et al. ball milled pure vanadium with different milling agents that reacted with the metal and altered the microstructure [17]. Hout et al. produced $TiV_{0.9}Mn_{1.1}$ by ball milling [18], while Lototsky could obtain ferrovanadium [19]. Zhang et al. reported the synthesis of V-4Cr-4Ti powders by high-energy vibrating and planetary ball milling [20]. The density of dislocation of powders synthesized by planetary ball milling was much lower than in specimens produced by vibrating ball milling at a similar input energy [20]. Finally, Balcerzak investigated the structure and the hydrogen storage properties of $Ti_{2-x}V_x$ nanocrystalline alloys ($x = 0.5, 0.75, 1, 1.25, 1.5$) synthesized by shaker-type ball milling [21]. All samples had a BCC crystalline structure and $Ti_{1.5}V_{0.5}$ reached a hydrogen storage capacity of 3.67 wt% at room temperature [21]. However, it must be noted that a large part of the hydrogen is absorbed at pressure as low as 10^{-3} MPa [21].

In this work, we decided not to use reactive ball milling in order to avoid the possible irreversible sorption of hydrogen occurring at such a low pressures that it would be hard to release it in our vacuum system. Therefore, we used ordinary ball milling in an argon atmosphere to synthesize the $V_{85}Ni_{15}$ sample, which was afterwards characterized by X-ray diffraction (XRD), energy dispersive X-ray analysis (EDX) and sorption measurements in a Sieverts apparatus.

2. Materials and Methods

V (99.5% purity, 325 mesh) and Ni (99.99% purity, 150 μ m diameter) powders were purchased from Sigma Aldrich. About 1.34 g of V and 0.26 g of Ni were manually mixed and transferred into an Evico Magnetic high-pressure vial. Ten stainless steel spheres with a diameter of 10 mm and a mass of 4.06 g were each added to the vial. All the previous procedures were performed in an argon-filled glove box. The powders were ball milled in a planetary Fritsch Pulverisette 6 at a rotation speed of 300 rpm during 30 cycles consisting of 30 min of milling and 10 min rest. The produced powders were removed from the vial in the argon-filled glove box to avoid contaminations from water and oxygen.

About 0.766 g of the milled powders were transferred in the glove box to the sample holder of a Sieverts apparatus. Smaller quantities were transferred to the sample holder for X-ray diffraction and SEM–EDX analysis.

Scanning electron micrographs were recorded by using a field emission scanning electron microscope (FESEM Auriga, Carl ZEISS, Oberkochen, Germany) at the CNIS research center.

X-ray diffraction (XRD) analysis was performed by using a Malvern Panalytical X'Pert Pro MPD diffractometer (Malvern Panalytical Ltd, Malvern, UK) equipped with a Ni-filtered Cu K α source ($\lambda = 1.54184 \text{ \AA}$) and an ultrafast RTMS X'Celerator detector (Malvern Panalytical Ltd, Malvern, UK). Measurements were carried out in the 10–80-degree range with a 0.01° step and an effective time/step = 15 s. Diffraction patterns were analyzed by Rietveld refinement program GSAS-II [22].

Hydrogen pressure-composition isotherms were measured by means of a homemade Sieverts apparatus, that can operate from room temperature up to 500°C in the pressure range between 10^{-4} to 200 bar, using various pressure transducers. The powders were initially heated at 170°C and exposed to a hydrogen pressure of 17 bar twice and dehydrogenated by means of turbopump that can produce a final vacuum on the order of 10^{-8} bar in the Sieverts apparatus. The quantity of hydrogen absorbed already in the first cycle coincides with that afterwards obtained during the more detailed investigation by pressure-composition curves. Therefore, it seems that the sample did not need an activation procedure at high temperatures, as the $\text{V}_{85}\text{Ni}_{15}$ sample produced by induction melting had to be activated at 400°C . Materials were collected from the Sievert apparatus after H_2 exchange in the glove box and analyzed by XRD and SEM–EDX.

3. Results and Discussion

3.1. Stoichiometric and Structural Analysis

The pristine V-Ni sample obtained after ball milling is constituted by micrometric secondary particles (see Figure 1a). An SEM analysis at high magnification highlights the presence of secondary particles of typical dimensions of a few microns, each of them composed of primary particles in the nanometer size scale (see Figure 1b).

The composition of the pristine sample obtained from the EDX point analysis on five different areas of the sample at different magnifications is reported in Table 1.

Table 1. Elemental analysis obtained from EDX before and after H_2 exchange. Nominal composition $\text{V}_{85}\text{Ni}_{15}$ with V/Ni nominal ratio of 5.7.

Element	Pristine	After H_2 Exchange 2
V	88 ± 5	87 ± 6
Ni	12 ± 5	13 ± 6
V/Ni ratio	7.0	6.6

The composition of the pristine alloy matches, as expected, the nominal alloy within the errors, being the experimental composition $\text{V}_{88\pm 5}\text{Ni}_{12\pm 5}$. Small amounts of iron have been found randomly distributed throughout the sample with a maximum experimental concentration below a few percent: this contamination originates from the ball-milling procedure.

The elemental distribution throughout the sample is shown in Figure 2, where the EDX emission maps for the L-edges of Ni (Figure 2b) and V (Figure 2c) are compared to the corresponding secondary electron micrography (Figure 2a).

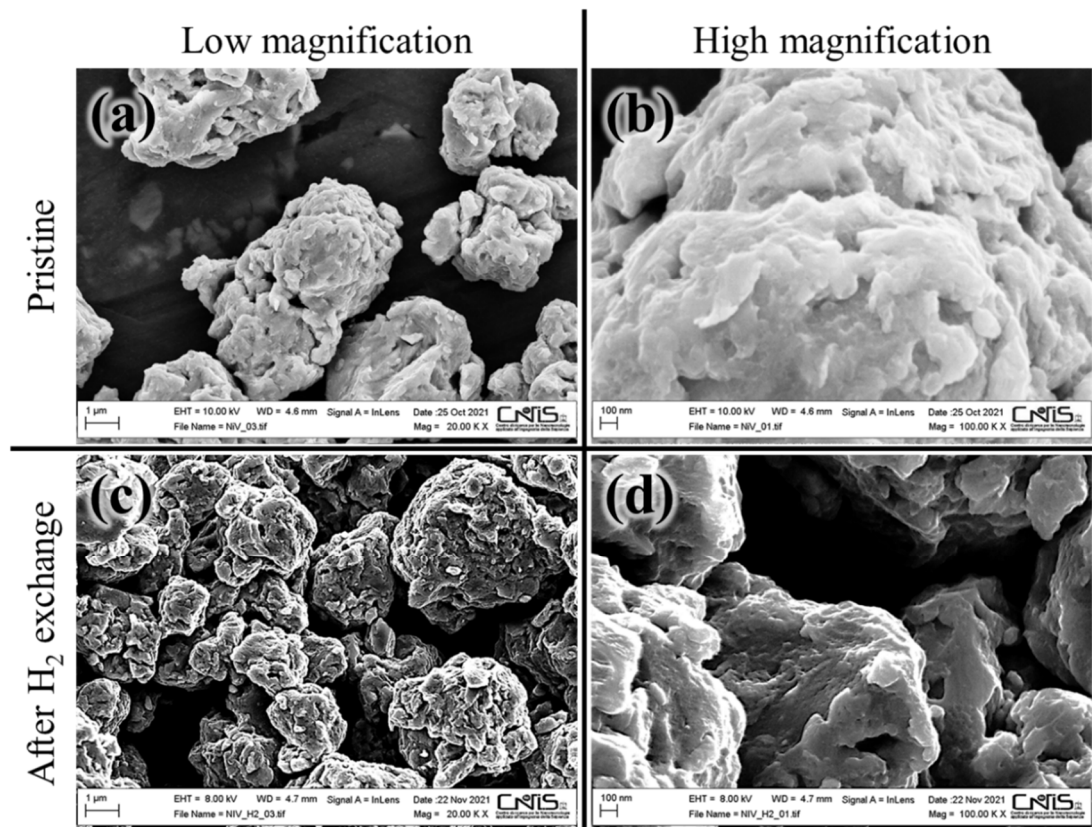


Figure 1. Electron micrographs of the pristine (a,b) and after H₂ exchange (c,d) samples, at low (a,c) or high (b,d) magnification.

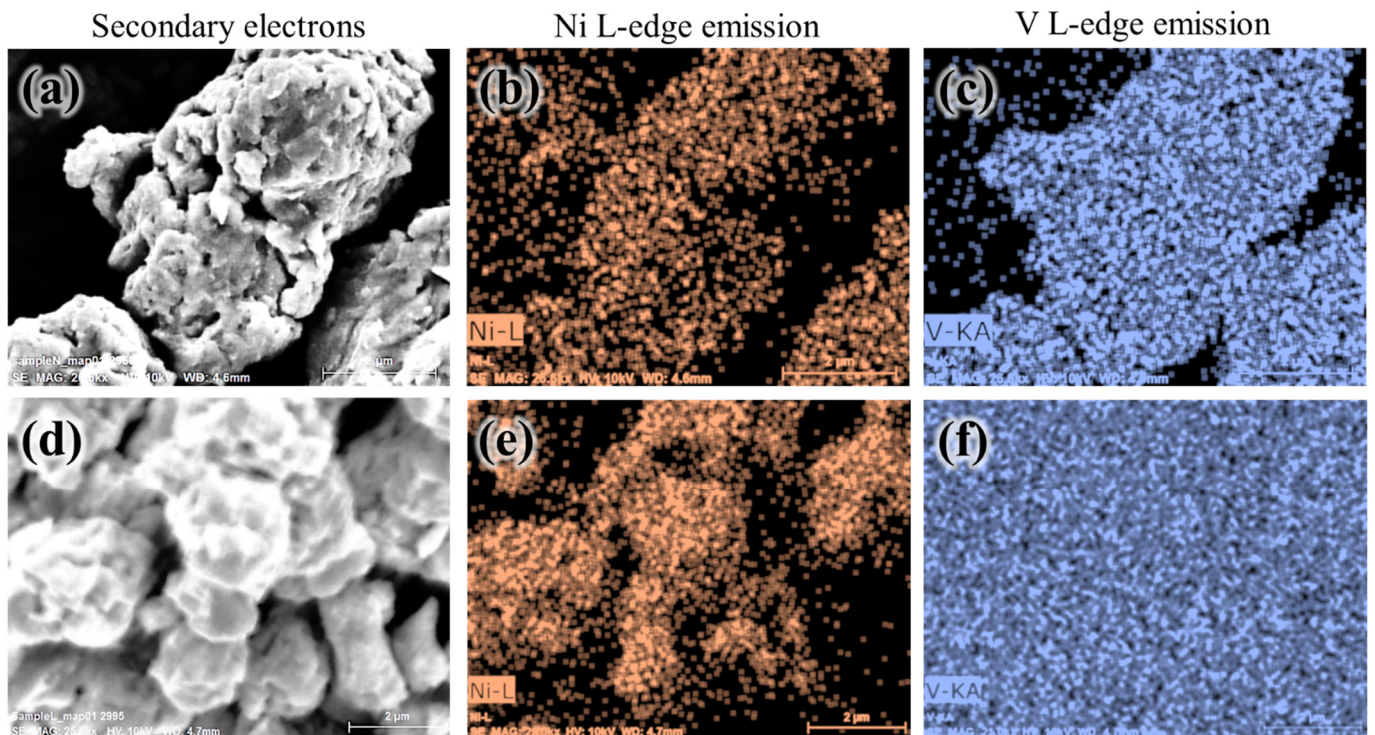


Figure 2. SEM micrographs and EDX maps of the V and Ni X-ray emissions at the L-edges (a–c) before and (d–f) after H₂ exchange.

Apparently, V and Ni are homogeneously distributed over the secondary particle surface, thus suggesting the alloy formation and the absence of elemental phase segregation. It is to be noted that the Ni X-ray signal is unavoidably much smaller compared to the vanadium signal: this inevitably imposes a balance between the definitions of the elemental maps and matching with micrographs (see as examples the poor special resolution of the Ni map in Figure 2b, or the special saturation of the V map in Figure 2f. The successful synthesis of a homogeneous V-Ni alloy is confirmed by XRD as well as the lack of extended phase contamination (see Figure 3).

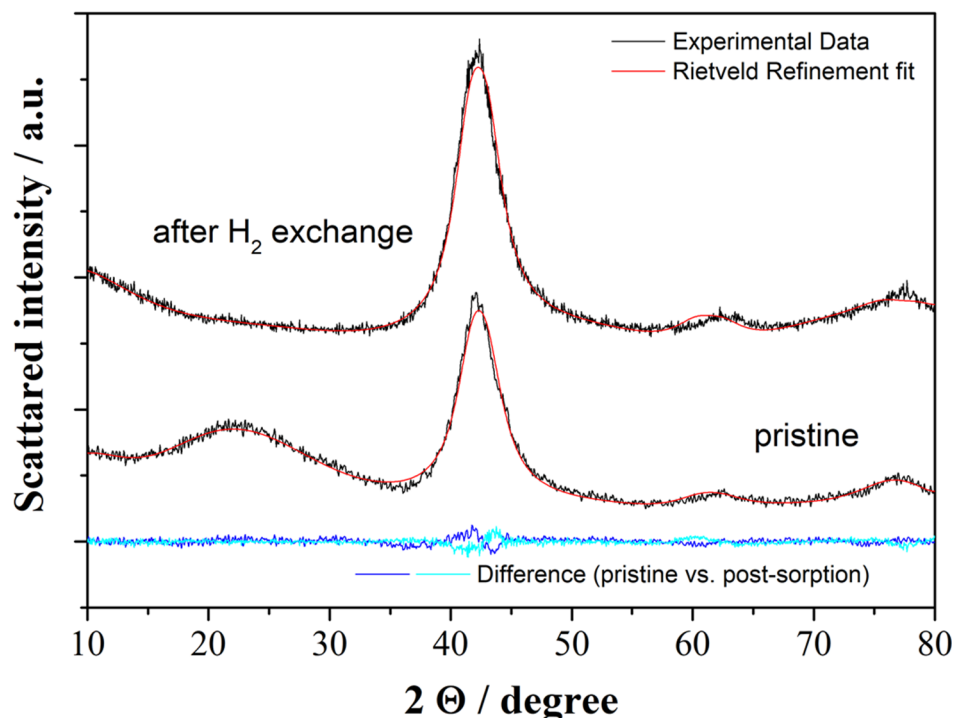


Figure 3. X-ray diffraction patterns before and after H₂ sorption compared to the Rietveld refinement fits and experimental-to-fitting difference lines.

The as-synthesized pristine sample shows in the XRD pattern few broad peaks and undulations of the baseline. This experimental feature suggests the lack of an extended crystallinity and the complete demolition of the pristine metals crystal structure by the mechanochemical treatment. The three strongest broad signals at about 41, 62 and 77 degrees can be indexed with Bragg reflections with Miller indexes (110), (200) and (211), possibly attributed to a body-centered-cubic (BCC) lattice, in line with our previous observation on a similar stoichiometry [11,12], and the attributions performed by other authors [7,21]. The broad undulation at 22–24 degrees has an apparent poor matching with any V-Ni ordered phase [11,12], and thus can be attributed to the glass sample holder or nanometric traces of V₂O₅.

The Rietveld refinement performed on the XRD pattern, assuming a BCC lattice with atomic sites randomly occupied by V and N as well as the experimental stoichiometry, confirms the qualitative analysis of the XRD pattern. The refinement procedure is in line with our previous approaches already reported in refs [11,12] and limits the fitting to three independent parameters (cubic lattice size, crystallite size and crystallite strain). The Rietveld refinement results are summarized in Table 2.

Table 2. Rietveld refinement results obtained on the pristine sample and after H₂ exchange. We assumed a single BCC lattice with a random occupancy of the atomic sites by Ni and V, mimicking the experimental stoichiometry.

	Pristine	After H ₂ Exchange
$a/\text{\AA}$	2.99 ± 0.01	3.05 ± 0.01
Size/nm	3.3 ± 0.1	4.9 ± 0.1
wRp	8.6%	8.3%
Gof	1.4	1.5

A good fitting is obtained assuming a single BCC phase with a 2.99 Å lattice parameter and a nanometric crystalline size of about 3.3 nm. Minor improvements in the fitting convergence (from 8.6 to 8.1%) can be obtained by adding a secondary BCC lattice with a slightly larger lattice parameter (i.e., 3.06 Å) to take into account the slight asymmetry in the peak shape towards small angles. Despite the fitting improvement, in our opinion the real co-presence of two alloys is too speculative solely based on the Rietveld refinement: in this view, the single-phase description is more conservative, although it possibly misses some minor structural features. It is interesting to underline that the primary crystallites are strongly nanometric with estimated size of 3.3 nm (see Table 2), a value that is very large compared to the polycrystalline particles observed by SEM (see Figures 1 and 2). This evidence suggests the possible massive occurrence of grain boundary defects between individual crystallites. Transmission electron microscopy experiments in future work may shed light on this specific morphological detail.

The V-Ni alloys synthesized by ball milling were submitted to extended H₂ exchange treatment at high temperature (see next section) to analyze their stability to store interstitial hydrogen and the sorption kinetics. After H₂ exchange, powders were collected in a charged state with a residual hydrogen content of H/M \approx 0.25 and characterized by XRD and SEM-EDX to highlight the most relevant changes induced by hydrogen incorporation/deincorporation. As expected, after H₂ exchange the V-Ni mechanochemical alloy shows:

- (a) An almost unaltered morphology (see Figure 1c,d);
- (b) A constant composition in terms of V/Ni ratio (see Table 1) with a homogeneous distribution of elements over the secondary particles (see Figure 2d–f);
- (c) The lack of new phase formation or additional nanosizing of the BCC phase (see Figure 3).

The most relevant change in the sample after H₂ exchange is the slight increase in the BCC lattice parameter fitted by Rietveld refinement (i.e., from 2.99 to 3.05 Å), and the increase in the crystal domain size for 3.3 to 4.9 nm (see Table 2). This lattice expansion is expected, as the sample was left in a state with a residual hydrogen content of H/M \approx 0.25. Furthermore, at a high temperature and under H₂ atmosphere, smaller crystallites have a tendency to sinter, thus inducing an increase in the overall crystallinity of the sample.

3.2. Hydrogen Absorption/Desorption

The hydrogen pressure-composition isotherms were measured at 120, 140 and 170 °C in the pressure range between 10^{−4} and 50 bar (see Figure 4). In general, the sample displays a decrease in the hydrogen solubility at a given pressure as temperature increases. Moreover, one can observe a quasi-linear dependence of the equilibrium pressure from hydrogen concentration up to H/M \approx 0.08, when reported in a double logarithmic scale. Therefore, at such low hydrogen concentration, p is proportional to (H/M) ^{m} , with $m \approx 2.7 \pm 0.1$ at 145 and 170 °C. This functional dependence of pressure on the hydrogen concentration, corresponds to a generalized Sieverts law with an exponent slightly different from 2 [23]. This fact seems to support the occurrence of a solid solution of hydrogen in the V-Ni alloy, without the formation of a hydride at low H/M in the temperature range between 120 and 170 °C [24].

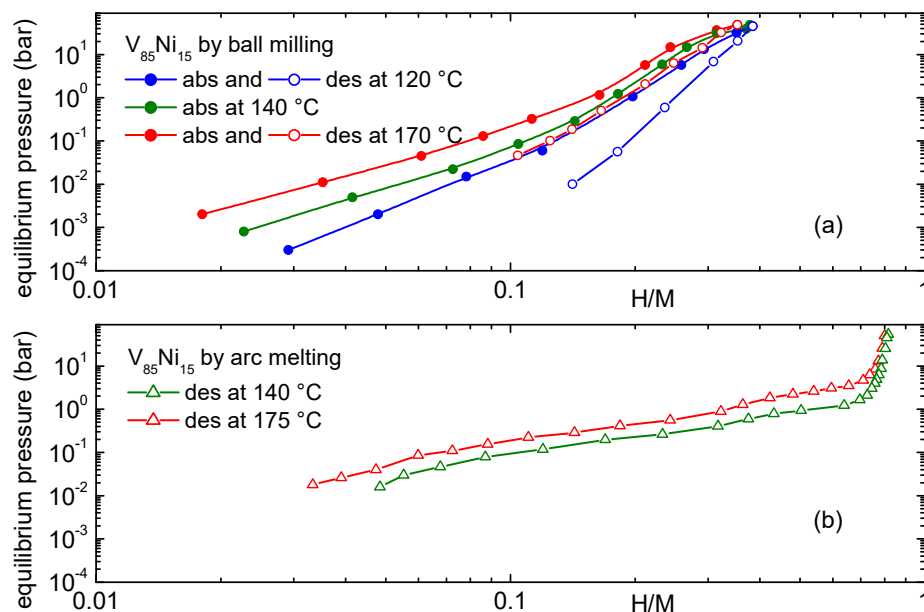


Figure 4. Panel (a): Absorption (full circles) and desorption (empty circles) pressure-composition isotherms at selected temperatures of ball-milled $V_{85}Ni_{15}$. Panel (b): desorption pressure-composition isotherms measured on $V_{85}Ni_{15}$ synthesized by arc melting [11] (empty triangles).

The shape of the isotherms of ball-milled $V_{85}Ni_{15}$ at low hydrogen concentrations is quite different from those of pure V. In fact, it was reported that in pure V, the Sieverts law is valid up to $H/M \sim 0.03$ [3] for temperatures between 92 and 190 °C. At higher hydrogen concentrations, one observes a clear pressure plateau for $0.03 < H/M < 0.5$; for $T < 140$ °C, the plateau is practically horizontal, while it becomes sloping between 160 and 190 °C. This plateau is due to the transition to the $VH_{0.5}$ hydride phase and the equilibrium pressure is quite low, as it is ~ 1 Torr (1.33×10^{-3} bar) at 190 °C. Previous studies of V alloys showed that the horizontal plateau of V for $H/M < 0.3$ becomes a sloping non-linear curve in alloys obtained by the addition of 6 at% of Mn, Fe, Co or Ni or 10 at% of Ti [5]; however, the equilibrium pressures are on the order of 10^{-4} bar at 70 °C [5].

Above $H/M \approx 0.08$, the equilibrium pressure of ball-milled $V_{85}Ni_{15}$ starts to deviate from the Sieverts law, and one can speculate that the sample will reach a pressure plateau above the maximum pressure investigated here ($p \sim 45$ bar). The shapes of the absorption and desorption isotherms are clearly different from those of $V_{85}Ni_{15}$ previously synthesized by arc melting, which are reported for comparison in Figure 4 at the same temperatures of those obtained for the ball-milled sample. In the sample synthesized by arc melting one observes an initial linear increase in the pressure as a function of H/M in a double logarithmic scale below $H/M \sim 0.08$ [11,25]. At higher concentrations, two different slopes are evident, for $0.1 < H/M < 0.3$ and for $0.4 < H/M < 0.6$ [11]. These findings were previously interpreted as evidence of the occurrence of a solid solution of H in the alloy for $H/M < 0.08$ (α phase), and the subsequent transformation of two different hydride phases, called β_1 and β_2 [11]. These hydrides have different dehydrogenation enthalpies: $\Delta H_{\text{dehydr}} = 21 \pm 1$ kJ/mol for $0.15 \leq H/M \leq 0.30$ and $\Delta H_{\text{dehydr}} = 26 \pm 2$ kJ/mol for $0.53 \leq H/M \leq 0.59$ [11]. It was reported that, above 300 °C, there is no evidence for the formation of hydrides in $V_{85}Ni_{15}$ produced by arc melting and only an α phase is present up to the maximum measured composition, with a hydrogenation enthalpy $\Delta H_{\text{hydr}} = 10.0 \pm 0.5$ kJ/mol [11].

From the hydrogen absorption curves of ball-milled $V_{85}Ni_{15}$ one can calculate the enthalpy and entropy changes during the hydrogenation by means of a Van't Hoff plot, reporting the logarithm of the equilibrium pressure as a function of the inverse of the absolute temperature and fitting the data by a linear regression. Usually, this method is applied to materials showing almost horizontal plateau pressures; however, it can also

be applied to materials with sloping equilibrium pressure, provided that the equilibrium pressures at fixed hydrogen compositions are analyzed [26,27].

Figure 5 reports the Van't Hoff plot of ball-milled $V_{85}Ni_{15}$ at four H/M values: 0.03, 0.06, 0.10, 0.20 and 0.25, together with the best fit lines. From the slope and intercept of the best fit, one can calculate the enthalpy and entropy variations during the hydrogenation process, as reported in Table 3. Both ΔH and ΔS decrease as the hydrogen concentration increases. In particular, ΔH passes from 90 ± 10 kJ/mol for H/M = 0.03 to 33 ± 4 kJ/mol at H/M = 0.20; concomitantly, ΔS decreases from 160 ± 30 J/(mol K) for H/M = 0.03 to 87 ± 9 J/(mol K) at H/M = 0.20. The values obtained for H/M = 0.25 have a very large uncertainty, and therefore, will not be further considered. The ΔH values are much higher than those obtained for $V_{85}Ni_{15}$ produced by arc melting ($\Delta H_{dehydr} = 21 \pm 1$ kJ/mol for $0.15 \leq H/M \leq 0.30$ and $\Delta H_{dehydr} = 26 \pm 2$ kJ/mol for $0.53 \leq H/M \leq 0.59$) [11]. Moreover, they are different from those of pure vanadium. Most information on pure V is available for the transformation toward the dihydride, VH_2 : Ono reported a ΔH of 49.4 kJ/mol [28], while Reilly reported a ΔH of 40 ± 1 kJ/mol [29]. Liu et al. measured the ΔH and ΔS of about 39.6 kJ/mol and 120 J/(mol K) for pure V and revealed that these values tended to decrease with a partial replacement of V by 3 at% of Al, Mn e Ru [6]. Griffiths et al. reported the enthalpy variation for the hydrogenation of pure vanadium for a low hydrogen content (H/M < 0.03) in the α (solid solution) phase. In this case, for H/M = 0.01 $\Delta H = 67.6 \pm 0.8$ kJ/mol [3]. However, Griffiths et al. showed that ΔH and ΔS increase (as absolute values) as the hydrogen concentration increases [3].

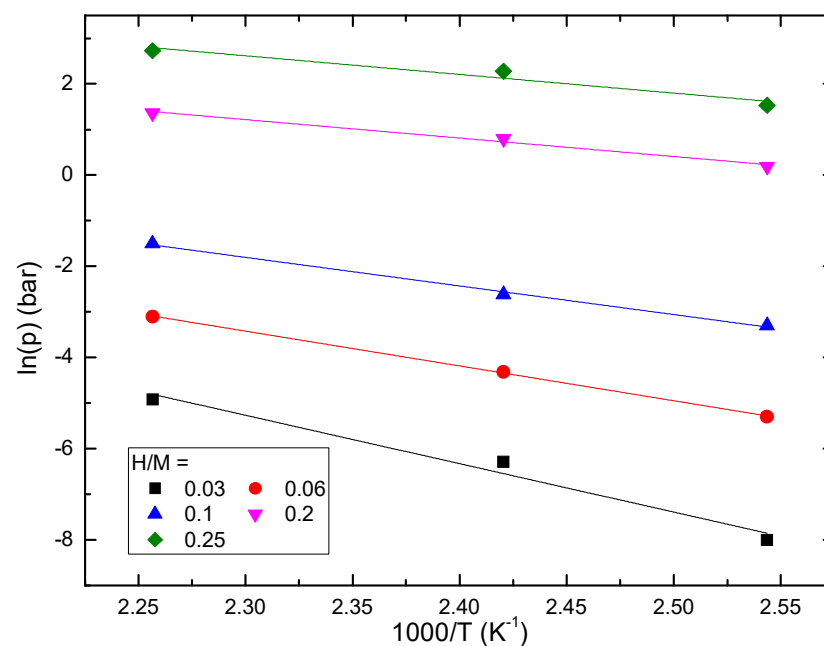


Figure 5. Van't Hoff plot of ball-milled $V_{85}Ni_{15}$ at selected H/M (the number of hydrogen atoms per atom of metal) and best fit lines to calculate the hydrogenation enthalpy.

Table 3. Hydrogenation enthalpy and entropy of ball-milled $V_{85}Ni_{15}$ as a function of the hydrogen concentration in the sample, expressed as H/M (the number of hydrogen atoms per atom of metal).

H/M	ΔH_{hyd} (kJ/mol)	ΔS_{hyd} (J/mol K ⁻¹)
0.03	90 ± 10	160 ± 30
0.06	63 ± 1	117 ± 3
0.10	52 ± 3	105 ± 7
0.20	33 ± 4	87 ± 9
0.25	34 ± 7	100 ± 20

Concerning the decrease in H with increasing hydrogen concentration, we can speculate here that, at the beginning of the hydrogenation process, the deepest hydrogen energy level becomes occupied; therefore, a large value of ΔH is measured. With the progression of hydrogenation, only shallower energy levels are left available; therefore, ΔH decreases. This effect was observed in some other hydrogen absorbing alloys based on Ni and Nb [27,30]. Regarding the entropy variation during the hydrogenation process, it must be said that entropy can change when a site blocking effect is present in the model. In this case, the presence of one hydrogen atom in interstitial sites of the metal lattice prevents other hydrogen atoms from occupying next-neighbor interstitial sites [31]. Some other cases of entropy variations with hydrogenation were reported for magnetic systems, such as $\text{LaFe}_{11.4}\text{Si}_{1.6}\text{H}_{1.6}$ [32], where a large change in the phonon density occurs during hydrogenation, and consequently, a large variation of the lattice entropy is observed.

All of the previous results on the ball-milled $\text{V}_{85}\text{Ni}_{15}$ sample display clear differences with those reported for V or $\text{V}_{85}\text{Ni}_{15}$ synthesized by induction melting. Although we do not have a clear explanation for these effects, we can speculate that they originate from the nanometric dimension of the powders produced here, which seem to hinder the formation of the β_1 and β_2 hydrides detected in pure V [1] and in $\text{V}_{85}\text{Ni}_{15}$ synthesized in a bulk crystalline form [11,12].

A final remark concerns the kinetics of hydrogen absorption. Figure 6 reports a comparison of the time evolution of hydrogen absorption at the three investigated temperatures (120, 140 and 170 °C) expressed as normalized capacity, starting from a common initial pressure of about 0.12 bar. As expected, the kinetics becomes faster at a higher temperature, and indeed, 95% of the maximum capacity can be reached in about 3300, 2400 and 1600 s at 120, 140 and 170 °C, respectively. These values are lower than that of pure activated LaNi_5 , a well-known material for hydrogen storage at room temperature, but are higher than those of non-activated LaNi_5 [33].

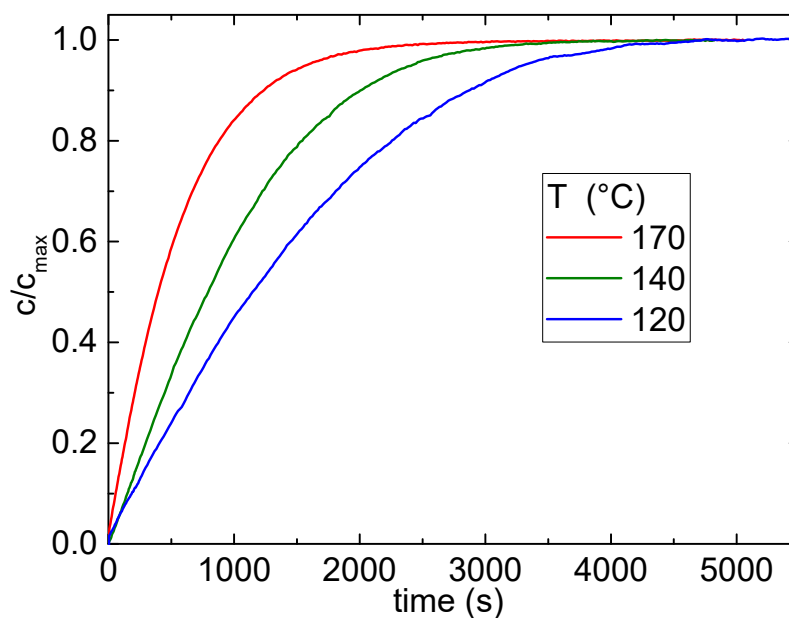


Figure 6. Kinetics of hydrogen absorption of ball-milled $\text{V}_{85}\text{Ni}_{15}$ at various temperatures expressed as the normalized capacity of the sample.

4. Conclusions

A $\text{V}_{85}\text{Ni}_{15}$ alloy was synthesized by ball milling the powders of the pure metals for 15 h in an argon atmosphere. SEM–EDX analyses confirmed the desired composition and indicate that the sample is composed of micrometric secondary particles due to the coalescence of primary particles of nanometric dimensions. X-ray diffraction measurements confirm a BCC structure of the crystalline phase, which has a mean size on the order of

3 nm. After hydrogenation, the crystalline phase is retained, the lattice parameter slightly increases, and the crystalline size expands to ≈ 5 nm.

From a functional point of view, ball-milled powders can absorb hydrogen without any activation procedure, up to a hydrogen content of $H/M \approx 0.4$ at the maximum pressure of ≈ 45 bar investigated here. Up to $H/M \approx 0.08$, the occurrence of a solid solution of hydrogen is observed, followed by the transition to a hydride upon increased hydrogen charging. Both the hydrogenation enthalpy and entropy decrease (as absolute values) with increasing hydrogen concentrations. The shape of the absorption isotherms is different from those obtained for $V_{85}Ni_{15}$ compound obtained by induction melting, possibly because of the nanometric dimensions of the powders produced by ball milling. Moreover, the isotherms were clearly different from those of pure V, which should present a very low pressure plateau up to $H/M \approx 0.5$ and the transition to dihydride, with a formal composition of VH_2 .

Author Contributions: Conceptualization, O.P. and A.P.; validation, O.P., N.C., F.T., S.B. and A.P.; formal analysis, N.C., S.B. and A.P.; investigation, O.P., N.C., F.T., S.B. and A.P.; resources, F.T.; writing—original draft preparation, A.P. and S.B.; visualization, N.C., S.B. and A.P.; supervision, A.P. All authors have read and agreed to the published version of the manuscript.

Funding: The authors would like to acknowledge the University of Rome La Sapienza for the funding through the project MA21916B755D01C9.

Data Availability Statement: Data are contained within the article.

Conflicts of Interest: The authors declare no conflict of interest.

References

1. Smith, J.F.; Peterson, D.T. The H-V (Hydrogen-Vanadium) System. *Bull. Alloy Phase Diagr.* **1982**, *3*, 55–60. [[CrossRef](#)]
2. Ukita, S.; Ohtani, H.; Hasebe, M. Thermodynamic analysis of the V–H binary phase diagram. *Mater. Trans.* **2008**, *49*, 2528–2533. [[CrossRef](#)]
3. Griffiths, R.; Pryde, J.A.; Righini-Brand, A. Phase diagram and thermodynamic data for the hydrogen/vanadium system. *J. Chem. Soc. Faraday Trans. 1* **1972**, *68*, 2344–2349. [[CrossRef](#)]
4. Otani, N.; Kuwabara, A.; Ogawa, T.; Fisher, C.J.A.; Tanaka, I.; Akiba, E. Equilibrium hydrogen pressures in the V–H system from first principles. *Int. J. Hydrogen Energy* **2019**, *44*, 28909–28918. [[CrossRef](#)]
5. Yukawa, H.; Yamashita, D.; Ito, S.; Morinaga, M.; Yamaguchi, S. Alloying effects on the phase stability of hydrides formed in vanadium alloys. *Mater. Trans.* **2002**, *43*, 2757–2762. [[CrossRef](#)]
6. Liu, Z.; Xiong, L.; Li, J.; Liu, S.; Er, S. Effects of alloying elements (Al, Mn, Ru) on desorption plateau pressures of vanadium hydrides: An experimental and first-principles study. *Int. J. Hydrogen Energy* **2018**, *43*, 21441–21450. [[CrossRef](#)]
7. Nakamura, Y.; Akiba, E. Hydriding properties and crystal structure of NaCl-type mono-hydrides formed from Ti–V–Mn BCC solid solutions. *J. Alloys Comp.* **2002**, *345*, 175–182. [[CrossRef](#)]
8. Steward, S.A. *Review of Hydrogen Isotope Permeability through Metals*. U.S. National Laboratory Report: UCRL-53441; Lawrence Livermore National Lab: Livermore, CA, USA, 1983.
9. Santucci, A.; Tosti, S.; Basile, A. Chapter 4. Alternatives to palladium in membranes for hydrogen separation: Nickel, niobium and vanadium alloys, ceramic supports for metal alloys and porous glass membranes. In *Handbook of Membrane Reactors*; Basile, A., Ed.; Woodhead Publishing Series in Energy; Woodhead Publishing: Cornwall, UK, 2013; Volume 1, p. 183e217. ISBN 978-0-85709-414-8.
10. Ockwig, N.W.; Nenoff, T.M. Membranes for Hydrogen Separation. *Chem. Rev.* **2007**, *107*, 4078–4110. [[CrossRef](#)]
11. Tosti, S.; Santucci, A.; Pietropaolo, A.; Brutti, S.; Palumbo, O.; Trequattrini, F.; Paolone, A. Hydrogen sorption properties of $V_{85}Ni_{15}$. *Int. J. Hydrogen Energy* **2018**, *43*, 2817–2822. [[CrossRef](#)]
12. Brutti, S.; Tosti, A.; Santucci, A.; Paolone, A. Deuterium absorption properties of $V_{85}Ni_{15}$ and evidence of isotope effect. *Int. J. Hydrogen Energy* **2019**, *44*, 20145–20149. [[CrossRef](#)]
13. Dunlap, R.A.; Cheng, Z.H.; MacKay, G.R.; O'Brien, J.W.; Small, D.A. Preparation of nanocrystalline metal hydrides by ball milling. *Hyperfine Interact.* **2000**, *130*, 109–126. [[CrossRef](#)]
14. Huot, J.; Cuevas, F.; Deledda, S.; Edalati, K.; Filinchuk, Y.; Grosdidier, T.; Hauback, B.C.; Heere, M.; Jensen, T.R.; Latroche, M.; et al. Mechanochemistry of Metal Hydrides: Recent Advances. *Materials* **2019**, *12*, 2778. [[CrossRef](#)] [[PubMed](#)]
15. Huot, J.; Ravnsbæk, D.B.; Zhang, J.; Cuevas, F.; Latroche, M.; Jensen, T.R. Mechanochemical synthesis of hydrogen storage materials. *Prog. Mater. Sci.* **2013**, *58*, 30–75. [[CrossRef](#)]
16. Orimo, S.-I.; Kimmerle, F.; Majer, G. Hydrogen in nanostructured vanadium-hydrogen systems. *Phys. Rev. B* **2001**, *63*, 094307. [[CrossRef](#)]

17. Krishnan, V.K.; Sinnaeruvadi, K. Synthesis of nanostructured vanadium powder by high-energy ball milling: X-ray diffraction and high-resolution electron microscopy characterization. *Philos. Mag. Lett.* **2016**, *96*, 402–408. [[CrossRef](#)]
18. Huot, J.; Enoki, H.; Akiba, E. Synthesis, phase transformation, and hydrogen storage properties of ball-milled TiV_{0.9}Mn_{1.1}. *J. Alloys Compds.* **2008**, *453*, 203–209. [[CrossRef](#)]
19. Lototsky, M.; Goh, J.; Davids, M.W.; Linkov, V.; Khotseng, L.; Ntsendwana, B.; Denys, R.; Yartys, V.A. Nanostructured hydrogen storage materials prepared by high-energy reactive ball milling of magnesium and ferrovandium. *Int. J. Hydrogen Energy* **2019**, *44*, 6687–6701. [[CrossRef](#)]
20. Zhang, Y.F.; Li, R.R.; Zhao, X.L.; Diao, S.Z.; Liu, P.P.; Wan, F.R.; Zhan, Q. Particle size evolution of V–4Cr–4Ti powders in high energy vibrating and planetary ball milling. *Mater. Res. Express* **2019**, *6*, 066535. [[CrossRef](#)]
21. Balcerzak, M. Structure and hydrogen storage properties of mechanically alloyed Ti–V alloys. *Int. J. Hydrogen Energy* **2017**, *42*, 23698–23707. [[CrossRef](#)]
22. Toby, H.H.; Von Dreele, R.B. GSAS-II: The genesis of a modern open-source all purpose crystallography software package. *J. Appl. Cryst.* **2013**, *47*, 544–549. [[CrossRef](#)]
23. Caravella, A.; Hara, S.; Drioli, E.; Barbieri, G. Sieverts law pressure exponent for hydrogen permeation through Pd-based membranes: Coupled influence of non-ideal diffusion and multicomponent external mass transfer. *Int. J. Hydrogen Energy* **2013**, *38*, 16229–16244. [[CrossRef](#)]
24. Sieverts, A. The Absorption of Gases by Metals. *Z. Für Met.* **1929**, *21*, 37–46.
25. Voyt, A.; Sidorov, N.; Sipatov, I.; Dobrotvorskii, M.; Piven, V. Hydrogen solubility in V₈₅Ni₁₅ alloy. *Int. J. Hydrogen Energy* **2017**, *42*, 3058–3063. [[CrossRef](#)]
26. Karger, B.L.; Snyder, L.R.; Horvath, C. *An Introduction to Separation Science*; Wiley: New York, NY, USA, 1973.
27. Palumbo, O.; Trequattrini, F.; Pal, N.; Hulyalkar, M.; Sarker, S.; Chandra, D.; Flanagan, T.; Dolan, M.; Paolone, A. Hydrogen absorption properties of amorphous (Ni_{0.6}Nb_{0.4–y}Ta_y)_{100–x}Zr_x membranes. *Prog. Nat. Sci.* **2017**, *27*, 126–131. [[CrossRef](#)]
28. Ono, S.; Nomura, K.; Ikeda, Y. The reaction of hydrogen with alloys of vanadium and titanium. *J. Less-Common Met.* **1980**, *72*, 159–165. [[CrossRef](#)]
29. Reilly, J.J.; Wiswall, R.H., Jr. The higher hydrides of vanadium and niobium. *Inorg. Chem.* **1970**, *9*, 1678–1682. [[CrossRef](#)]
30. Jayalakshmi, S.; Choi, Y.G.; Kim, Y.C.; Kim, Y.B.; Fleury, E. Hydrogenation properties of Ni–Nb–Zr–Ta amorphous ribbons. *Intermetallics* **2010**, *18*, 1988–1993. [[CrossRef](#)]
31. Zepon, G.; Hessel Silva, B.; Zlotea, C.; Botta, W.J.; Champion, Y. Thermodynamic modelling of hydrogen-multicomponent alloy systems: Calculating pressure-composition-temperature diagrams. *Acta Mater.* **2021**, *215*, 117070. [[CrossRef](#)]
32. Terwey, A.; Gruner, M.E.; Keune, W.; Landers, J.; Salamon, S.; Eggert, B.; Ollefs, K.; Brabänder, V.; Radulov, L.; Skokov, K.; et al. Influence of hydrogenation on the vibrational density of states of magnetocaloric LaFe_{11.4}Si_{1.6}H_{1.6}. *Phys. Rev. B* **2020**, *101*, 064415. [[CrossRef](#)]
33. Todorova, S.; Abrashev, B.; Rangelova, V.; Mihaylov, L.; Vassileva, E.; Petrov, K.; Spassov, T. Hydrogen Gas Phase and Electrochemical Hydriding of LaNi_{5–x}M_x (M = Sn, Co, Al) Alloys. *Materials* **2021**, *14*, 14. [[CrossRef](#)]